

## Developing with lethal RA levels: genetic ablation of *Rarg* can restore the viability of mice lacking *Cyp26a1*

Suzan Abu-Abed<sup>1</sup>, Pascal Dollé<sup>2</sup>, Daniel Metzger<sup>2</sup>, Caroline Wood<sup>1</sup>, Glenn MacLean<sup>1</sup>, Pierre Chambon<sup>2</sup> and Martin Petkovich<sup>1,\*</sup>

<sup>1</sup>Cancer Research Labs, Queen's University, Kingston, ON K7L 3N6, Canada

<sup>2</sup>Institut de Génétique et de Biologie Moléculaire et Cellulaire, Collège de France, BP 163-67404 Illkirch Cedex, CU de Strasbourg, France

\*Author for correspondence (e-mail: petkovic@post.queensu.ca)

Accepted 16 December 2002

### SUMMARY

We have previously reported that the retinoic acid (RA) catabolizing enzyme CYP26A1 plays an important role in protecting tail bud tissues from inappropriate exposure to RA generated in the adjacent trunk tissues by RALDH2, and that *Cyp26a1*-null animals exhibit spina bifida and caudal agenesis. We now show that, in the absence of *Cyp26a1*, retinoic acid receptor gamma (RAR $\gamma$ ) mediates ectopic RA-signaling in the tail bud. We also show that activated RAR $\gamma$  results in downregulation of *Wnt3a* and *Fgf8*, which integrate highly conserved signaling pathways known for their role in specifying caudal morphogenesis.

Ablation of the gene for RAR $\gamma$  (*Rarg*) rescues *Cyp26a1*-null mutant animals from caudal regression and embryonic lethality, thus demonstrating that CYP26A1 suppresses the RA-mediated downregulation of WNT3A and FGF8 signaling pathways by eliminating ectopic RA in gastrulating tail bud mesoderm.

Key words: Gastrulation, Tail bud, Cytochrome P450, Homeotic transformations, Mouse mutant, Retinoids, Retinoic acid, Teratogenesis, Spina bifida, Caudal regression, *Cyp26a1*, RAR $\gamma$ , *Wnt3a*, *Brachyury*, *Fgf8*, *Hnf3b*, *Cdx4*, *Hoxd11*, *Tbx6*, *Raldh2*

### INTRODUCTION

Retinoic acid (RA), a biologically active metabolite of vitamin A (retinol), is a signaling molecule required for normal embryogenesis. RA signaling is mediated by nuclear RA receptors (RARs –  $\alpha$ ,  $\beta$ ,  $\gamma$  – and their isoforms; and RXRs –  $\alpha$ ,  $\beta$ ,  $\gamma$ ) (reviewed by Chambon, 1996) and depends on the coordinated expression of specific synthesizing (RALDH1, RALDH2 and RALDH3) (Mic et al., 2000; Niederreither et al., 2002b) and catabolizing (CYP26A1, CYP26B1) (Abu-Abed et al., 1998; Fujii et al., 1997; MacLean et al., 2001) enzymes, whose actions specify RA distribution patterns throughout the developing embryo. Gastrulation, a process whereby the early embryo is converted from two germ layers into three (ectoderm, mesoderm and endoderm) and the anteroposterior axis is defined (Beddington and Robertson, 1999), is vulnerable to perturbations in RA signaling caused by either genetic or nutritional means. *Raldh2* and *Cyp26a1* knockout and expression studies indicate that the tightly regulated synthesis and distribution of RA is especially crucial during late stages of gastrulation (Abu-Abed et al., 2001; Fujii et al., 1997; Niederreither et al., 1997; Niederreither et al., 1999; Sakai et al., 2001).

Although RA is undetectable during the early stages of gastrulation (E6.5-E7.5) (Rossant et al., 1991; Ulven et al., 2000), *Cyp26a1* is expressed in the primitive streak and its newly formed mesoderm (Fujii et al., 1997). The onset of

*Raldh2* expression at E7.5 complements that of *Cyp26a1*, which shifts from the posterior embryo to all three germ layers of the anterior half. At this stage, ingressing epiblast cells may encounter a pool of RA, generated by *Raldh2*, in newly formed mesoderm that surrounds the primitive streak and node region (Niederreither et al., 1997; Rossant et al., 1991), and predominantly contributes to somite formation (Kinder et al., 1999). A state of RA deficiency generated by loss of RALDH2 activity leads to severe developmental defects that affect late-streak-derived structures, such as the trunk somites, heart and limbs (Niederreither et al., 1999). By contrast, exposure to teratogenic doses of RA at E7.5 affects development of more anterior structures, such as the face and brain (Iulianella and Lohnes, 1997; Simeone et al., 1995). During this stage, CYP26A1 may protect anterior structures from RA exposure, as some *Cyp26a1*-null animals exhibit exencephaly (Abu-Abed et al., 2001).

During late gastrulation (E8.5-E10), *Cyp26a1* expression shifts posteriorly, becoming mainly restricted to the open neuropore, hindgut endoderm and tail bud mesoderm. Thus, the domain of *Cyp26a1* expression in the tail bud abuts that of *Raldh2* in the trunk mesoderm, a complementarity that persists until somitogenesis is complete (~E13). Tissues derived from the tail bud at this stage include paraxial mesoderm of the lumbosacral region, and, to a lesser extent, lateral plate mesoderm, notochord, posterior neural tube and hindgut (Kinder et al., 1999). In the absence of CYP26A1 function,

assays involving a RA-responsive *lacZ* reporter transgene reveal that tail bud tissues normally devoid of RA stain positively for RA activity (Sakai et al., 2001). Loss of CYP26A1 function is embryonic lethal, with mutant embryos dying from caudal regression associated with spina bifida, imperforate anus, agenesis of the caudal portions of the digestive and urogenital tracts, malformed lumbosacral skeletal elements, and lack of caudal tail vertebrae (Abu-Abed et al., 2001; Sakai et al., 2001). This phenotype indicates that CYP26A1 is also essential for maintaining morphogenetic events during late gastrulation, probably by protecting tail bud tissues from exposure to RA.

The caudal regression phenotype of *Cyp26a1* mutants closely resembles that of wild-type embryos treated with teratogenic doses of RA at E8.5-E9.5 (Alles and Sulik, 1990; Kessel, 1992; Padmanabhan, 1998). Such RA-treated wild-type embryos show elevated levels of apoptosis, develop ectopic neural tubes and exhibit severe downregulation of *Wnt3a* expression in tail bud tissues (Alles and Sulik, 1990; Iulianella et al., 1999; Shum et al., 1999; Yasuda et al., 1990). Interestingly, loss of WNT3A function leads to a caudal regression syndrome similar to that observed in *Cyp26a1* mutants and RA-treated wild-type embryos (Takada et al., 1994). Finally, resistance to the teratogenic effects of RA has been observed in mice that lack *Rarg*, which develop caudal tissues normally and show no change in *Wnt3a* expression after RA treatment during late gastrulation (Lohnes et al., 1993; Iulianella et al., 1999). Based on these observations, we were interested in testing whether we could rescue *Cyp26a1* mutants from endogenous RA teratogenicity by disrupting the *Rarg* gene.

We report that loss of *Rarg* rescues *Cyp26a1* mutants from embryonic lethality and suppresses their caudal regression phenotype. Furthermore, ablation of *Rarg* restores normal gene expression patterns in the tail bud of *Cyp26a1*<sup>-/-</sup>*Rarg*<sup>-/-</sup> double mutants. Our results suggest that RA signaling mediated by RAR $\gamma$  downregulates WNT3A and FGF8 signaling activities, leading to defects in caudal mesoderm and definitive endoderm formation. Using this double mutant model, not only do we better dissect the biological role of CYP26A1 in late gastrulation and tail bud development, but we also show that it is possible to suppress the lethal effects of one null mutation by introducing another, a phenomenon as yet rarely observed in mouse.

## MATERIALS AND METHODS

### Animals and genotyping

The *Cyp26a1*<sup>-/-</sup> and *Rarg*-null mice used in this study have been previously described (Abu-Abed et al., 2001; Iulianella and Lohnes, 1997). *Cyp26a1*<sup>+/-</sup>*Rarg*<sup>+/-</sup> animals were mated overnight and females examined the following morning for the presence of a vaginal plug; noon of the day of plug was considered as embryonic day (E) 0.5. Pregnant females were sacrificed by cervical dislocation and embryos or fetuses were collected in sterile phosphate-buffered saline (PBS). Yolk sacs were used for genotyping by PCR. The following three primers were used to amplify 200 and 350 bp fragments from the *Cyp26a1* wild-type and mutant alleles, respectively: 5' CTGGGCTGAAGGTGGGATAAGTGTCCCTC 3', 5' CCACGTCCACTCTGCTATGCTGTTGAGCATCAGCTG 3' and 5' GAAGATATCTGCCACATCGTGGGTGTCACAGATAC 3'. The

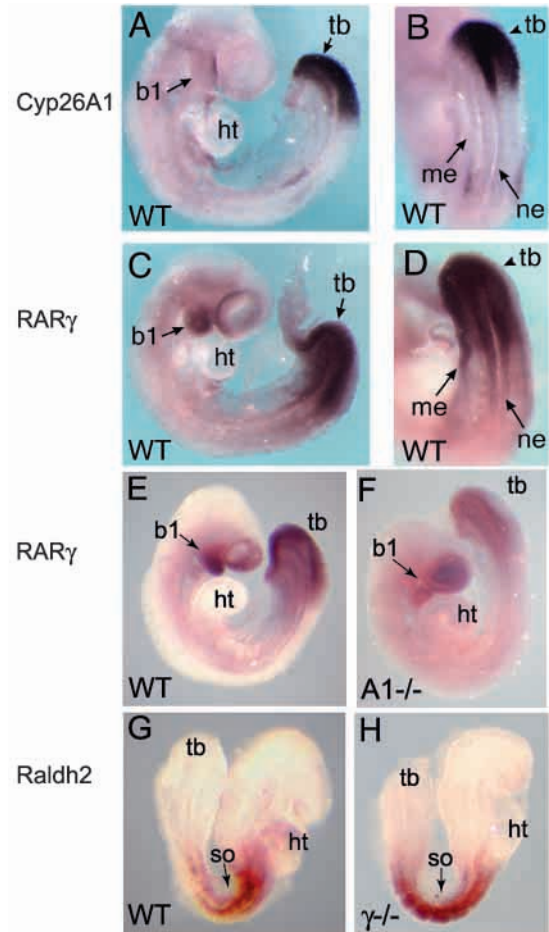


**Fig. 1.** *Cyp26a1*, *Rarg* and *Raldh2* expression in wild-type and mutant embryos. Comparative views of E9.0 wild-type (WT) embryos, after hybridization with *Cyp26a1* (A,B) and *Rarg* (C,D) riboprobes. Profile views (A,C) and detail of the caudal region (B,D). Note the differential extent of both types of transcripts, *Rarg* extending more rostrally than *Cyp26a1* in both mesodermal (me) and neuroectodermal (ne) tissues. (E,F) *Rarg* transcript distribution in E9.0 wild-type (E) and *Cyp26a1*<sup>-/-</sup> (F) embryos. Although the overall *Rarg* expression level may be decreased (e.g. in the first branchial arches, b1), its spatial distribution does not appear to be altered in the mutant. (G,H) *Raldh2* exhibits comparable transcript distributions in E8.0 wild-type (G) and *Rarg*<sup>-/-</sup> (H) embryos. b1, first branchial arch; ht, heart; so, somites; tb, tail bud.

following two primers were used to amplify a 120 bp fragment from the *Rarg* wild-type allele: 5' CAGAGCACCAGCTCGGAGGA 3' and 5' CTTCACAGGAGCTGACCCCA 3'. In a separate reaction, a primer complementary to the 5' coding region of the *Neo* gene, 5' GGCCGGAGAACCCTGCGTGCAATCC 3', was used in combination with the first *Rarg* primer to amplify ~700 bp fragment from the mutant allele. The PCR conditions used were as follows: 94°C for 30 seconds, 55°C (*Cyp26a1*) or 60°C (*Rarg*) for 30 seconds, and 72°C for 1 minute for 30 cycles.

### Skeletal analysis

Fetuses were skinned, eviscerated, and dehydrated in 100% ethanol. Carcasses were stained with 0.03% Alcian Blue in 80% ethanol:20% glacial acetic acid to detect cartilaginous elements. Specimens were then dehydrated in 100% ethanol, cleared overnight in 1% potassium hydroxide, and stained overnight in 0.1% Alizarin Red S in 1%

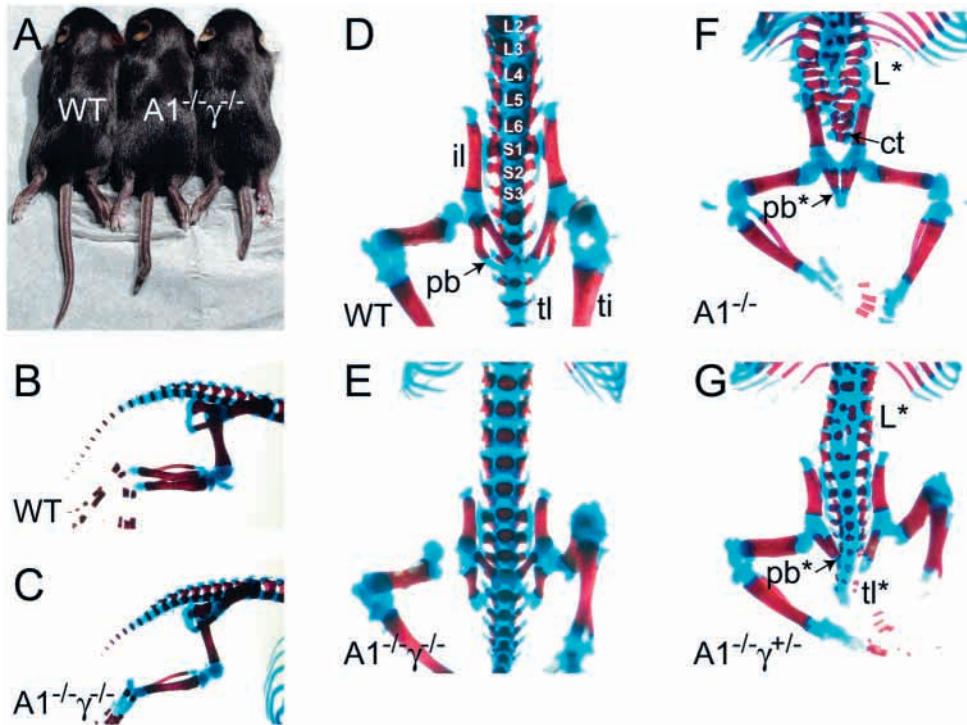


**Fig. 2.** A *Rarg*-null mutant background rescues the *Cyp26a1*-null mutant caudal phenotype. In comparison to a wild-type littermate (A, left), two 10-day-old *A1*<sup>-/-</sup>*γ*<sup>-/-</sup> double mutants (A, right) show kinked and/or shortened tails. Compared with a wild-type skeleton (B) at E18.5, an *A1*<sup>-/-</sup>*γ*<sup>-/-</sup> (C) skeleton reveals that the tail vertebrae have a normal morphology, although tail development is reduced by approximately four vertebral condensations. The wild-type skeleton (D) exhibits six lumbar (L1-L6; L1 not shown), three fused sacral (S1-S3) and caudal tail (tl) vertebrae. The ilium (il) articulates with S1 and the pelvic bone (pb), which articulates with the hindlimbs. While the skeleton of the *A1*<sup>-/-</sup>*γ*<sup>-/-</sup> mutant (E) is comparable with that of the wild-type animal, the *A1*<sup>-/-</sup> (F) and *A1*<sup>-/-</sup>*γ*<sup>+/-</sup> (G) mutants develop abnormally; both skeletons show deformed and abnormally fused lumbar vertebrae (L\*), with the *A1*<sup>-/-</sup> mutant being more severely affected. Furthermore, in the *A1*<sup>-/-</sup>*γ*<sup>+/-</sup> mutant,

the malformed pelvic bone (pb\*) is connected to abnormally twisted hindlimbs and only six rudimentary caudal vertebrae contribute to the tail (tl\*). The *A1*<sup>-/-</sup> mutant exhibits a similarly deformed pelvic bone and twisted hindlimbs, as well as a more severe caudal truncation (ct), developing only three sacral rudiments.

potassium hydroxide. Clearing was achieved by several changes of 20% glycerol in 1% potassium hydroxide over 1 week, followed by 50% glycerol:50% ethanol for 2-3 weeks. Specimens were scored under a dissecting microscope and photographed with a digital camera.

#### In situ hybridization analysis

Staged embryos were pooled by genotype and rehydrated in a methanol series. *Brachyury*, *Cdx4*, *Fgf8*, *Hnf3b*, *Hoxd11*, *Tbx6* and *Wnt3a* probes were kindly provided by Drs B. Herrmann, J. Deschamps, G. Martin, S.-L. Ang, D. Duboule, V. Papaioannou and A. McMahon, respectively. Whole-mount in situ hybridization was performed according to Wilkinson (Wilkinson, 1992). After hybridization, embryos were cleared and photographed under a dissecting scope (Leica MZ 9.5) with a digital camera.

## RESULTS

### *Cyp26a1* and *Rarg* are co-expressed in embryonic caudal tissues

The relationship between *Cyp26a1* and *Rarg* expression domains was analyzed by comparative whole-mount in situ hybridization of wild-type E9 embryos (Fig. 1A-D). *Cyp26a1* exhibits strong and specific expression within the tail bud neuroepithelium and mesoderm (Fig. 1A,B) has been previously reported (Fujii et al., 1997; Abu-Abed et al., 2001; MacLean et al., 2001). *Rarg* transcripts were also markedly expressed in the caudal region of the embryo (Fig. 1C-E). However, these transcripts were not as sharply restricted as those of *Cyp26a1* and extended up to slightly more rostral

levels, both within the posterior neuroepithelium and the lateral mesoderm (compare Fig. 1B with 1D). In E9.0 embryos, *RARG* expression was not compromised by *Cyp26a1* ablation (compare Fig. 1E with 1F). At this stage, there were no obvious changes in tissue morphology in the *Cyp26a1*<sup>-/-</sup> mutants when compared with wild-type littermates. Because we have previously observed that reducing *Raldh2* expression can result in rescue of the *Cyp26a1*<sup>-/-</sup> caudal defect (Niederreither et al., 2002a), we also wanted to establish whether *Raldh2* expression was normal in *Rarg* mutants. Fig. 1G,H shows that *Raldh2* expression levels are not decreased in *Rarg*-null embryos.

### A *Rarg*-null mutant background rescues *Cyp26a1* mutants from embryonic lethality

*Cyp26a1*<sup>+/-</sup>*Rarg*<sup>+/-</sup> double heterozygous mutant mice were intercrossed to generate compound mutants. For simplicity, *Cyp26a1* and *Rarg* are abbreviated *A1* and *γ*, respectively (e.g. *A1*<sup>-/-</sup> and *A1*<sup>-/-</sup>*γ*<sup>-/-</sup> represent *Cyp26a1*<sup>-/-</sup> and *Cyp26a1*<sup>-/-</sup>*Rarg*<sup>-/-</sup> mutants, respectively). Embryos at E8.5-9.5, E18.5 fetuses and 10-day old newborn pups collected from *A1*<sup>+/-</sup>*γ*<sup>+/-</sup> intercrosses were considered for analysis of Mendelian ratios; specimens were also collected from *A1*<sup>+/-</sup>*γ*<sup>-/-</sup> females mated with *A1*<sup>+/-</sup>*γ*<sup>+/-</sup> males, in order to increase the yield of double mutant embryos and fetuses. At E8.5-9.5, *A1*<sup>-/-</sup>*γ*<sup>-/-</sup> embryos were collected at approximately a third of the expected ratio, while other genotypes were observed at the expected Mendelian ratios (Table 1). At E18.5, the *A1*<sup>-/-</sup>*γ*<sup>-/-</sup> and *A1*<sup>-/-</sup> genotypes were observed at two-thirds and one-third of the expected frequencies, respectively. At 10 days post-partum, *A1*<sup>-/-</sup>*γ*<sup>-/-</sup> mutants were observed at approx. half the

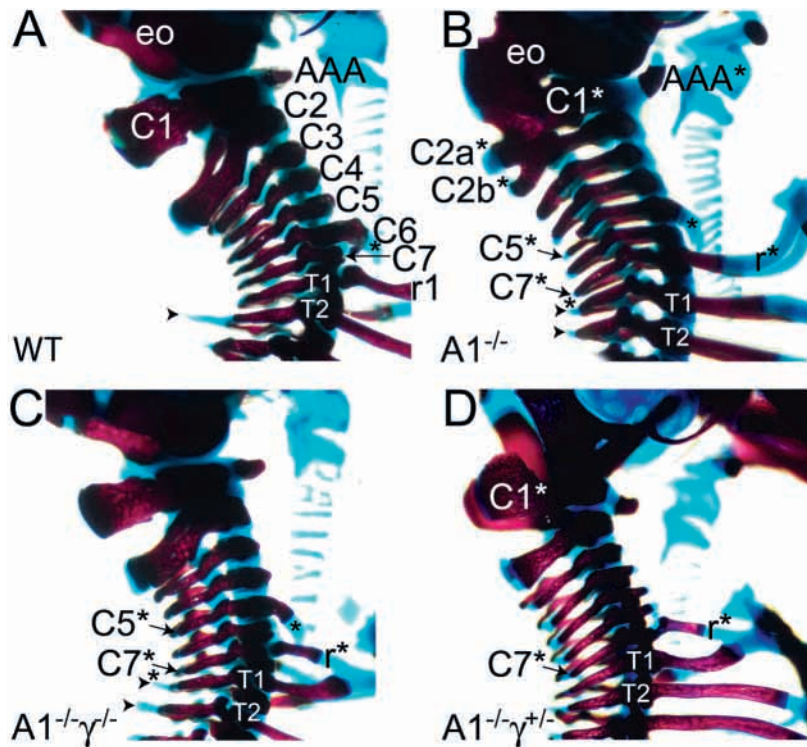


**Fig. 3.** A *Rarg*-null mutant background rescues a subset of the *Cyp26a1*<sup>-/-</sup> cervical vertebral abnormalities. In wild-type skeletons (A), the first cervical vertebra (C1 or atlas) develops a thick neural arch and an anterior arch (AAA); anterior tuberculi (\*) distinguish C6. Thoracic (T) vertebrae harbor ribs (see r1 on T1), the first seven of which articulate with the sternum. T2 vertebrae also develop a prominent dorsal spinous process (arrowhead). The *AI*<sup>-/-</sup> mutant skeleton (B) shows several posterior homeotic transformations (see Results), including C5 to C6 (C5\*), C7 to T1 (C7\*) and T1 to T2 (\*). In addition, the *AI*<sup>-/-</sup> mutant exhibits fusion between the exoccipital bone (eo) and the neural arch of C1 (C1\*), an abnormal AAA (AAA\*) and bifidus of C2 (C2a\* and C2b\*). Whereas posterior homeotic transformations are evident in the *AI*<sup>-/-</sup> mutant (C), including C5 to C6 (C5\*), C7 to T1 (C7\*) and T1 to T2 (\*) transformations, C1 and C2 develop normally. In the *AI*<sup>-/-</sup>γ<sup>+/-</sup> mutant (D), C7 exhibits a posterior transformation (C7\*); also, the neural arch of C1 and the exoccipital bone (eo) are fused.

expected ratio, distinguished in some cases by a shortened and/or kinked tail (Fig. 2A-C). No *AI*<sup>-/-</sup> or *AI*<sup>-/-</sup>γ<sup>+/-</sup> newborns were recovered 10 days post-partum. Altogether, these results suggest that a *Rarg*-null mutant background rescues approximately half of the *AI*<sup>-/-</sup> mutants from lethality. As *AI*<sup>-/-</sup>γ<sup>-/-</sup> mutants obtained at embryonic and fetal stages were externally indistinguishable from their wild-type counterparts, it is likely that the *AI*<sup>-/-</sup>γ<sup>-/-</sup> embryos not rescued by the *Rarg*-null background were resorbed before E8.5. Previously, we have recovered *Cyp26a1*<sup>-/-</sup> embryos exhibiting early lethality

(Abu-Abed et al., 2001). We have also found that exposing *Cyp26a1*<sup>-/-</sup> embryos to subteratogenic doses of RA at E7.5 increases early lethality (S. A.-A., P. D., D. M., C. W., G. M., P. C. and M. P., unpublished), suggesting that variations in maternal RA status results in variability in the expressivity of the *Cyp26a1*<sup>-/-</sup> phenotype. Lack of RARγ may make embryos more susceptible to this phenotype, possibly by potentiating inappropriate signaling through RARα or RARβ. We are currently attempting to characterize the cause of this early lethality. All generated *AI*<sup>-/-</sup>γ<sup>-/-</sup> animals continued to gain

**Table 1. Observed Mendelian ratios**

Genotype	Expected (%)	Observed (%)			Total (316)
		E8.5-9.5 (127)*	E18.5 (46)	PD10 (143)†	
Wild type	6.25	5.5 (7)	8.7 (4)	9.8 (14)	7.9 (25)
<i>AI</i> <sup>-/-</sup>	6.25	7.9 (10)	2.2 (1)	0	3.5 (11)
γ <sup>-/-</sup>	6.25	7.9 (10)	10.9 (5)	5.6 (8)	7.3 (23)
<i>AI</i> <sup>-/-</sup> γ <sup>-/-</sup>	6.25	2.4 (3)	4.3 (2)	3.5 (5)	3.2 (10)
<i>AI</i> <sup>-/-</sup> γ <sup>+/-</sup>	12.5	11.8 (15)	15.2 (7)	0	7.0 (22)
<i>AI</i> <sup>+/-</sup> γ <sup>-/-</sup>	12.5	8.7 (11)	13.0 (6)	11.9 (17)	10.8 (34)
<i>AI</i> <sup>+/-</sup>	12.5	11.0 (14)	10.9 (5)	18.9 (27)	14.5 (46)
γ <sup>+/-</sup>	12.5	14.9 (19)	8.7 (4)	15.4 (22)	14.2 (45)
<i>AI</i> <sup>+/-</sup> γ <sup>+/-</sup>	25	29.2 (38)	26.1 (12)	34.9 (50)	31.6 (100)

\*Numbers in parentheses indicate total number of specimens analyzed. All specimens identified in this table were collected from *AI*<sup>+/-</sup>γ<sup>+/-</sup> intercrosses. †PD10=postnatal day 10.

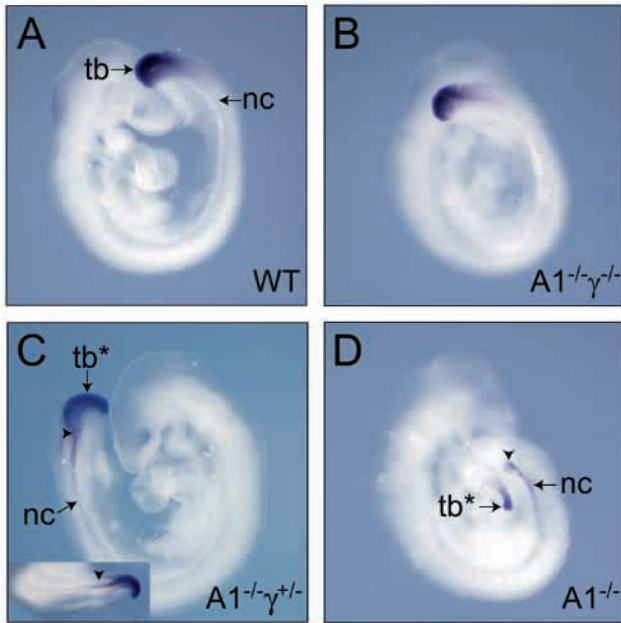


**Fig. 4.** Rescue of *Brachyury* expression in  $AI^{-/-}\gamma^{-/-}$  double mutant embryos. *Brachyury* expression patterns in the wild-type (A) and  $AI^{-/-}\gamma^{-/-}$  (B) embryos are comparable, showing strong expression in the tail bud (tb) nascent mesoderm and neuroepithelium, as well as the notochord (nc).  $AI^{-/-}\gamma^{+/-}$  (C) and  $AI^{-/-}$  (D) mutants show eversion and twisting of tissues caudal to the posterior neuropore (PNP, arrowhead). *Brachyury* expression is severely downregulated in the  $AI^{-/-}$  mutant tail bud ( $tb^*$ ), while notochord labeling stops abruptly at the level of the PNP (arrowhead).

weight at a rate similar to that of their wild-type offspring. However,  $AI^{-/-}\gamma^{-/-}$  females were apparently sterile, even after

a 3-month exposure to fertile males. The cause of this infertility is under investigation.

**The *Cyp26a1*-null mutant caudal regression syndrome is rescued in a *Rarg*-null background**

Previous analysis of *Cyp26a1*-null mutant embryos revealed that, in addition to malformed lumbosacral vertebrae and lack of caudal tail vertebrae,  $AI^{-/-}$  mutants suffer from an open posterior neuropore (spina bifida), as well as agenesis of the posterior urogenital and digestive systems (Abu-Abed et al., 2001; Sakai et al., 2001). The most severely affected  $AI^{-/-}$  mutants lack the entire caudal body and/or show various degrees of hindlimb fusions (sirenomelia). Skeletal phenotypes for both  $AI^{-/-}$  and  $\gamma^{-/-}$  null mutants have been previously described (Abu-Abed et al., 2001; Iulianella and Lohnes, 1997; Lohnes et al., 1993; Sakai et al., 2001) (see Table 2). Apart from the lumbosacral truncation and lack of tail vertebrae (Fig. 2F),  $AI^{-/-}$  mutants exhibit consistent abnormalities of cervical vertebrae, most of which correspond to posterior homeotic transformations (Table 2; Fig. 3B). On the other hand, a fraction of the  $\gamma^{-/-}$  mutants exhibit anterior transformations of cervical and thoracic vertebrae (Table 2, and data not shown).

We analyzed the vertebral patterns of  $AI^{-/-}\gamma^{-/-}$  double mutants at E18.5 [for a detailed description of the wild-type vertebral patterns, see Kessel (Kessel, 1992)]. The *Rarg*<sup>-/-</sup> background almost fully rescued *Cyp26a1*-null mutants from the caudal regression syndrome. In contrast to  $AI^{-/-}$  mutants (Fig. 2F),  $AI^{-/-}\gamma^{-/-}$  skeletons (Fig. 2C,E) exhibited six normal, evenly spaced lumbar, three normal sacral and 15 ossified caudal vertebrae, whereas wild-type littermates (Fig. 2B,D) had 18 ossified tail vertebrae. Furthermore,  $AI^{-/-}\gamma^{-/-}$  mutants had a normal pelvic bone and correctly set hindlimbs (compare Fig. 2B,D with 2C,E). We also examined the effects of *Rarg* haploinsufficiency by analyzing two E18.5  $AI^{-/-}\gamma^{+/-}$  mutants.

**Table 2. Summary of skeletal abnormalities**

	$AI^{-/-}\gamma^{-/-}$	$AI^{-/-}\gamma^{+/-}$	$AI^{-/-}$ *	$\gamma^{+/-}$
Vertebral malformations in cervical region				
Exoccipital-C1 neural arch fusion	-‡	+§	++¶	-
Exoccipital-C1 AAA fusion**	-	-	-	+
C1 bifidus	-	-	+	+
C2 bifidus	-	-	++	+
C1-C2 fusion	-	-	-	+
C2-C3 fusion	-	-	-	+
Tracheal rings fused/disrupted	+++†	-	-	+++
Posterior vertebral transformations				
C5 to C6	++	+++	++	-
C7 to T1	+++	+++	+++	-
T1 to T2	++	++	+++	-
Anterior vertebral transformations				
C2 to C1	-	-	-	+
C6 to C5	-	-	-	+
C7 to C6	-	-	-	+
T8 to T7	-	-	-	+
L1 to T13	-	++	++	-

\*Our previous (Abu-Abed et al., 2001) and present observations. †Lohnes et al., 1993; 8% of  $\gamma^{+/-}$  animals showed T8 to T7 transformations only. ‡Not observed. §Observed in less than half. ¶Observed in more than half. \*\*Anterior arch of atlas. ††Observed in all specimens.

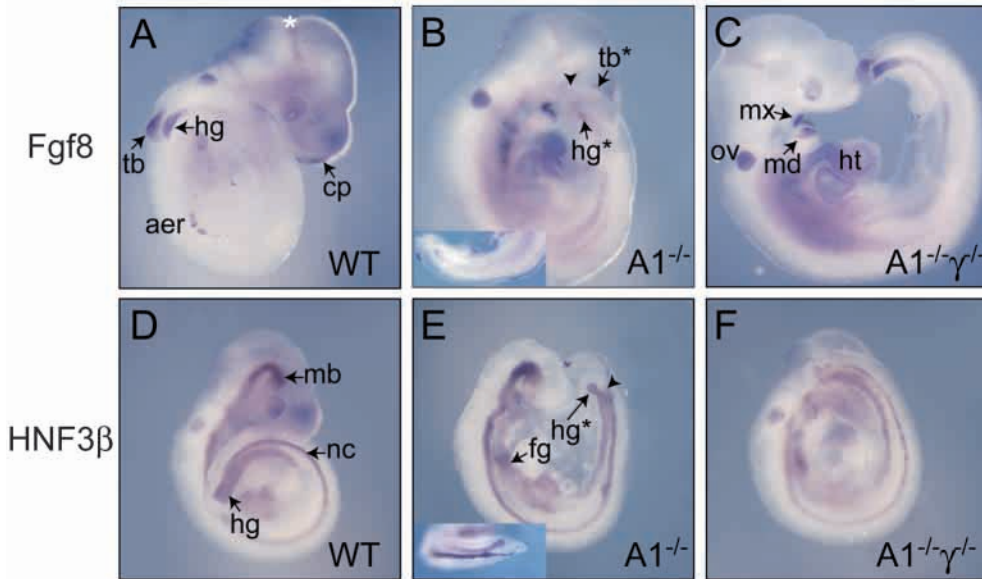


**Fig. 5.** *Fgf8* and *Hnf3b* expression patterns are rescued in the tail bud and hindgut of *AI*<sup>-/-</sup> $\gamma$ <sup>+/-</sup> mutants. *Fgf8* is normally (A) expressed in the midbrain-hindbrain junction (white asterisk), maxillary (mx) and mandibular (md) components of the first branchial arch, otic vesicle (ov), commissural plate (cp), heart (ht) and associated vasculature, hindgut (hg), and tail bud (tb) nascent mesoderm. (D) *Hnf3b* expression is specific of the midbrain (mb), notochord (nc), foregut (fg) and hindgut (hg). In the *AI*<sup>-/-</sup> mutant (B), *Fgf8* hindgut labeling (hg\*) stops at the level of the posterior neuropore (PNP, arrowhead) and expression is down-regulated in the nascent mesoderm of the malformed, twisted tail bud tissues (tb\*; see inset). Although *Hnf3b* notochord labeling persists in the everted tail bud tissues of the *AI*<sup>-/-</sup> mutant (E, inset), hindgut labeling ends at the level of the PNP (arrowhead). *AI*<sup>-/-</sup> $\gamma$ <sup>+/-</sup> double-mutants show normal *Fgf8* and *Hnf3b* patterns of expression (C and F, respectively). aer, apical ectodermal ridge.

Although one of these *AI*<sup>-/-</sup> $\gamma$ <sup>+/-</sup> skeletons (Fig. 2G) showed an intermediate phenotype with lumbosacral vertebrae less deformed than in *AI*<sup>-/-</sup> mutants and a truncated tail rudiment, the other showed fusion and twisting of the hindlimbs, as well as malformed lumbosacral region and no caudal tail vertebrae (data not shown). These results indicate that the rescue of *AI*<sup>-/-</sup> animals by *Rarg* haploinsufficiency is partial and not fully penetrant, possibly accounting for the absence of viable *AI*<sup>-/-</sup> $\gamma$ <sup>+/-</sup> animals in our crosses.

### Suppression of other vertebral abnormalities

We also examined whether loss of RAR $\gamma$  function may revert the *AI*<sup>-/-</sup> cervical phenotype (Table 2; Fig. 3). The first and second cervical vertebrae (C1 and C2) developed normally in all *AI*<sup>-/-</sup> $\gamma$ <sup>+/-</sup> mutants examined (Fig. 3C;  $n=4$ ). By contrast, one of the *AI*<sup>-/-</sup> skeletons showed fusion between the exoccipital bone and neural arch of C1, whereas both *AI*<sup>-/-</sup> skeletons exhibited this malformation (compare Fig. 3B with 3D). In addition, *AI*<sup>-/-</sup> skeletons generally showed bifidus of the neural arch on C2 (Fig. 3B). This latter phenotype is also observed in some of the  $\gamma$ <sup>-/-</sup> mutants (Lohnes et al., 1993; Lohnes et al., 1994). None of the *AI*<sup>-/-</sup> $\gamma$ <sup>-/-</sup> or *AI*<sup>-/-</sup> $\gamma$ <sup>+/-</sup> double mutants exhibited such malformations (Fig. 3C,D).

The *AI*<sup>-/-</sup> $\gamma$ <sup>-/-</sup>, *AI*<sup>-/-</sup> $\gamma$ <sup>+/-</sup> and *AI*<sup>-/-</sup> mutants showed the following posterior homeotic transformations within the C5-T1 region: a C5 to C6 transformation, which was demonstrated by the presence of unilateral or bilateral anterior tuberculi on C5, structures normally characteristic of C6 (2/4 *AI*<sup>-/-</sup> $\gamma$ <sup>-/-</sup>, 1/2 *AI*<sup>-/-</sup> $\gamma$ <sup>+/-</sup>, 2/2 *AI*<sup>-/-</sup>); a C7 to T1 transformation, as evidenced by the presence of ectopic ribs on C7 that were fused to either T1 or to the sternum (4/4 *AI*<sup>-/-</sup> $\gamma$ <sup>-/-</sup>, 2/2 *AI*<sup>-/-</sup> $\gamma$ <sup>+/-</sup>, 2/2 *AI*<sup>-/-</sup>); and a T1 to T2 transformation, indicated by the presence of a prominent ectopic spinous process on T1 in addition to the one normally observed on T2 (2/4 *AI*<sup>-/-</sup> $\gamma$ <sup>-/-</sup>, 1/2 *AI*<sup>-/-</sup> $\gamma$ <sup>+/-</sup>, 2/2 *AI*<sup>-/-</sup>) (compare Fig. 3A-D; see Table 2 for a summary). Thus, in contrast to the rescue of the C1-C2 abnormalities, it appears

that ablation of *Rarg* does not rescue the posterior transformations observed within the C5-T1 region of *AI*<sup>-/-</sup> mutants. Furthermore, the *AI*<sup>-/-</sup> $\gamma$ <sup>-/-</sup> and *AI*<sup>-/-</sup> $\gamma$ <sup>+/-</sup> compound mutants did not display anterior homeotic transformations normally observed in the cervicothoracic region of *Rarg*<sup>-/-</sup> mutants (Iulianella and Lohnes, 1997; Lohnes et al., 1993). Some *AI*<sup>-/-</sup> mutants showed an L1 to T13 transformation due to the development of unilateral or bilateral ectopic ribs on L1 (data not shown; Table 2). *AI*<sup>-/-</sup> $\gamma$ <sup>+/-</sup>, but not *AI*<sup>-/-</sup> $\gamma$ <sup>-/-</sup> compound mutants, also exhibited this anterior transformation. Finally, the tracheal rings were ventrally fused and disrupted in all *AI*<sup>-/-</sup> $\gamma$ <sup>-/-</sup> skeletons examined, a malformation also observed in all *Rarg*<sup>-/-</sup> mutants (Lohnes et al., 1993) (Table 2). Thus, not all defects resulting from *Cyp26a1* ablation are rescued by loss of RAR $\gamma$  function, suggesting that other RARs may compensate for ectopic RA signaling in the C5-T1 region.

### Normal expression of genes involved in tail bud morphogenesis is restored in E9.5 *Cyp26a1/Rarg* double null embryos

To characterize the molecular defects resulting from loss of CYP26A1 function, and their possible rescue by ablation of *Rarg*, we analyzed genes known for their specific expression in tail bud tissues and/or whose mutation generates developmental defects in the caudal region of the embryo. In situ hybridization experiments were carried out at E9.5, which corresponds to an early stage of tail bud growth in wild-type embryos, at which mild caudal defects are seen in the *AI*<sup>-/-</sup> embryos. Each expression pattern was analyzed on one *AI*<sup>-/-</sup> $\gamma$ <sup>-/-</sup> and two *AI*<sup>-/-</sup> $\gamma$ <sup>+/-</sup> compound mutants, in comparison with *AI*<sup>-/-</sup> and  $\gamma$ <sup>-/-</sup> single mutants, as well as wild-type control embryos processed in the same experimental series. As none of the expression patterns found in  $\gamma$ <sup>-/-</sup> mutant embryos differed from wild-type patterns, these mutants are not discussed further.

*Wnt3a* transcripts are expressed in the primitive streak,

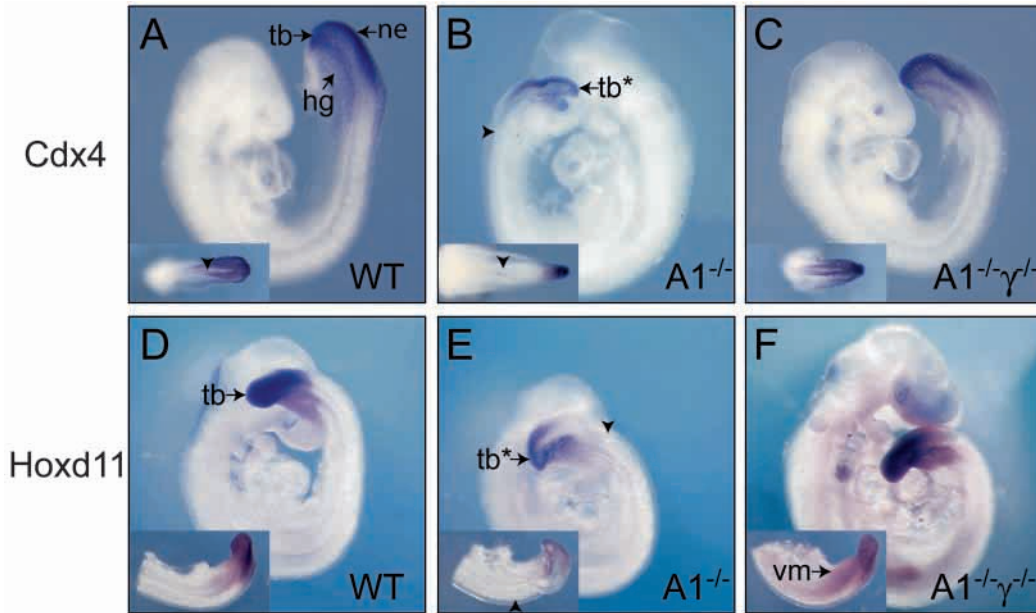


**Fig. 6.** *Cdx4* and *Hoxd11* expression patterns are downregulated in the tail bud of *AI*<sup>-/-</sup> mutants, but are restored in *AI*<sup>-/-</sup> $\gamma$ <sup>-/-</sup> mutants. *Cdx4* is expressed in a graded anteroposterior manner along the tail bud mesoderm (tb), hindgut (hg) and neuroepithelium (ne) of the wild-type embryo (A). *Hoxd11* shows prominent expression in tail bud (tb) mesoderm and neuroepithelium of the wild-type (D) embryo. In *AI*<sup>-/-</sup> mutants (B) *Cdx4* expression is downregulated in the tail bud (tb\*) mesoderm, neuroepithelium and hindgut (arrowhead indicates posterior neuropore). *AI*<sup>-/-</sup> embryos (E) also show downregulation of *Hoxd11* expression in the tail bud (arrowhead indicates last fully formed somite). *AI*<sup>-/-</sup> $\gamma$ <sup>-/-</sup> mutants exhibit normal *Cdx4* (C) and *Hoxd11* (F) expression, although, in comparison with the wild-type embryo (D inset), *Hoxd11* transcripts extend more rostrally along the ventral mesoderm (vm) (F, inset).

nascent mesoderm and neuroepithelium of the developing tail bud (Parr et al., 1993; Roelink and Nusse, 1991). *Wnt3a*-null embryos show defects caudal to the forelimbs in that they lack trunk somites, have a disrupted notochord and fail to form tail bud tissues (Takada et al., 1994). We (Abu-Abed et al., 2001) and others (Sakai et al., 2001) have previously examined the expression of *Wnt3a* in *Cyp26a1*-null mutants and found its expression to be downregulated within the nascent mesoderm and neuroepithelium. By contrast, the E9.5 *AI*<sup>-/-</sup> $\gamma$ <sup>-/-</sup> embryo expressed *Wnt3a* normally (data not shown). To substantiate these findings, we chose to examine a downstream target of WNT3A signaling, the T-box gene *Brachyury* (Herrmann et al., 1990).

As reported (Abu-Abed et al., 2001; Sakai et al., 2001), *AI*<sup>-/-</sup> embryos showed reduced *Brachyury* expression in the tail bud nascent mesoderm and neuroepithelium, whereas expression in the notochord indicated abnormal development of this structure (compare Fig. 4A with 4D). By contrast, *Brachyury* expression levels in the tail bud tissues of *AI*<sup>-/-</sup> $\gamma$ <sup>-/-</sup> (Fig. 4B) and *AI*<sup>-/-</sup> $\gamma$ <sup>+/-</sup> (Fig. 4C) compound mutants were comparable with those observed in wild-type littermates (Fig. 4A). Interestingly, while the *AI*<sup>-/-</sup> $\gamma$ <sup>-/-</sup> mutant displayed normal morphology (Fig. 4B), the *AI*<sup>-/-</sup> $\gamma$ <sup>+/-</sup> embryo was malformed caudally, showing eversion and twisting of tail bud tissues (Fig. 4C, inset). This malformation was also observed, albeit more severely, in the *AI*<sup>-/-</sup> mutant (Fig. 4D), indicating that restoration of *Brachyury* expression may not be sufficient to achieve normal development of tail bud tissues in compound mutants. These results confirm that down-regulation of WNT3A signaling in *AI*<sup>-/-</sup> mutants affects expression of a WNT3A downstream target.

*Fgf8*-null mutants also show severe gastrulation defects and lack several mesoderm- and endoderm-derived structures (Sun et al., 1999). *Fgf8* is expressed in the primitive streak, dorsal half of the nascent mesoderm, neuroepithelium and hindgut endoderm of the wild-type tail bud (Fig. 5A) (Crossley and Martin, 1995). *Fgf8* expression was virtually absent from the tail bud of *AI*<sup>-/-</sup> and *AI*<sup>-/-</sup> $\gamma$ <sup>+/-</sup> embryos, except for weak expression within the nascent mesoderm (Fig. 5B; inset, and data not shown). Furthermore, abnormal tail bud morphology

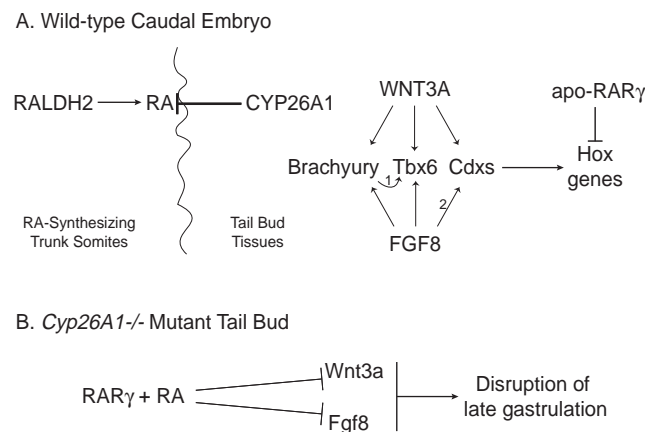


**Fig. 7.** RAR $\gamma$  mediates ectopic RA signaling in the tail bud, a genetic model. See Discussion for rationale. *Brachyury* is thought to maintain *Tbx6* expression (1) (Yamaguchi et al., 1999). Based on studies in *Xenopus*, FGF8 may play a role in regulating *Cdx* expression patterns (2).

of the  $AI^{-/-}$  mutant suggested minimal tissue development caudal to the posterior neuropore (PNP) in this particular embryo (Fig. 5B, inset). By contrast, *Fgf8* expression in the  $AI^{-/-}\gamma^{-/-}$  embryo was comparable with that of the wild-type embryo (compare Fig. 5A with 5C).

We examined the expression of an additional hindgut endoderm marker, *Hnf3b*, which is also expressed in the notochord and floor plate of the neural tube (Fig. 5D) (Ang et al., 1993; Monaghan et al., 1993; Sasaki and Hogan, 1993). *Hnf3b* expression persisted in the notochord and floor plate of  $AI^{-/-}$  and  $AI^{-/-}\gamma^{-/-}$  embryos (Fig. 5E; data not shown), although labeling indicated that both structures developed abnormally (Fig. 5E, inset; data not shown). In tail bud tissues caudal to the PNP, *Hnf3b* labeling also indicated a reduction in the size of the hindgut pocket, whose development appeared to stop prematurely in both  $AI^{-/-}$  and  $AI^{-/-}\gamma^{-/-}$  mutants (Fig. 5E; data not shown). Abnormal patterns of expression were not detected in the  $AI^{-/-}\gamma^{-/-}$  embryo (Fig. 5F; data not shown).

Loss of FGF signaling has been shown to disrupt expression of *caudal*-related genes in *Xenopus* (Northrop and Kimelman, 1994). As *Fgf8* was abnormally expressed in  $AI^{-/-}$  and  $AI^{-/-}\gamma^{-/-}$  embryos, we examined the expression of *Cdx4*, one of three known *caudal*-related genes in mouse (Gamer and Wright, 1993). *Cdx4* shows a rostrocaudal gradient of expression within tail bud tissues of E9.5 wild-type embryos, with its expression being most intense caudally (Fig. 6A). In  $AI^{-/-}$  mutant embryos, *Cdx4* expression was downregulated in both the neuroepithelium and nascent mesoderm of the tail bud, having an expression boundary that altogether shifted posteriorly (compare Fig. 6A with 6B, insets);  $AI^{-/-}\gamma^{-/-}$  mutants showed a less pronounced caudal shift (data not shown). *Cdx4* expression in the  $AI^{-/-}\gamma^{-/-}$  embryo was similar to that of wild-type littermates (compare Fig. 6A with 6C).

Pownall et al. (Pownall et al., 1996) have demonstrated that *caudal*-related transcription factors regulate the expression of Hox genes in *Xenopus*; similar observations have been made in the case of *Cdx1*-null mice (Subramanian et al., 1995). We chose to analyze the expression of *Hoxd11*, which together with other 5'-located Hox genes, is involved in setting up regional identities along the lumbosacral column and posterior urogenital and digestive structures (Favier and Dollé, 1997). *Hoxd11* is strongly expressed at E9.5 throughout most of the tail bud tissues, its expression being stronger towards the caudal extremity (Fig. 6D). *Hoxd11* expression was downregulated in the tail bud tissues of  $AI^{-/-}$  embryos, especially within the hindgut, presomitic and lateral mesoderm, and to a lesser extent in the neuroepithelium (Fig. 6E). Moreover,  $AI^{-/-}$  mutants showed comparably reduced expression domains of *Cdx4* and *Hoxd11* expression (compare Fig. 6B with 6E, insets), indicating that CDX4 may indeed regulate Hox gene expression. By contrast, *Hoxd11* expression levels in  $AI^{-/-}\gamma^{-/-}$  and  $AI^{-/-}\gamma^{-/-}$  compound mutants were comparable with those seen in wild-type embryos (Fig. 6F; and data not shown), although expression was expanded along the ventral mesoderm (compare Fig. 6D with 6F, insets; see Discussion).

## DISCUSSION

CYP26A1 is a highly conserved component of the RA signaling pathway, showing tail bud-specific expression in several vertebrate species, including mouse, chicken, *Xenopus* and zebrafish (de Roos et al., 1999; Fujii et al., 1997; Hollemann et al., 1998; Iulianella et al., 1999; MacLean et al., 2001; Swindell et al., 1999). *Cyp26a1*-null mutant mouse fetuses die from severe caudal defects that mimic RA teratogenicity (Alles and Sulik, 1990; Durston et al., 1997; Griffith and Wiley, 1991; Ruiz i Altaba and Jessell, 1991; Yasuda et al., 1990), suggesting that CYP26A1 protects the developing tail bud from ectopic RA signaling (Fig. 7A) (Abu-Abed et al., 2001; Sakai et al., 2001). Disruption of CYP26A1 activity allows RA generated in the differentiating trunk somites to diffuse into the tail bud, which ultimately disrupts mesoderm and definitive endoderm formation (Niederreither et al., 2002a; Sakai et al., 2001). We show that caudal development is rescued in *Cyp26a1*<sup>-/-</sup>*Rarg*<sup>-/-</sup> double-mutant animals, substantiated by the normal expression of molecular markers involved in tail bud morphogenesis. This provides evidence that the catabolic activity of CYP26A1 suppresses the teratogenic effects of ectopic RA signaling. Specifically, we have also demonstrated that RAR $\gamma$  mediates the deleterious effects of RA on caudal development by downregulating the critical signaling activities of WNT3A and FGF8 (Sun et al., 1999; Takada et al., 1994). Therefore, our results reveal the existence of an epistatic relationship between the *Cyp26a1* and *Rarg* gene functions. Fig. 7B summarizes a genetic model based on our present work and that of others.

### A *Rarg*-null background rescues most, but not all defects in *Cyp26a1*<sup>-/-</sup> animals

Although *Cyp26a1* and *Rarg* tail bud-expression patterns overlap in a spatiotemporal manner (Fujii et al., 1997; MacLean et al., 2001; Ruberte et al., 1990) (see Fig. 1), CYP26A1 is critical for normal caudal development whereas RAR $\gamma$  is dispensable (Abu-Abed et al., 2001; Lohnes et al., 1993; Look et al., 1995; Sakai et al., 2001). *Rarg*-null animals are viable, exhibiting vertebral transformations and malformations in the cervical region, in addition to squamous metaplasia and/or keratinization of various glandular epithelia. Moreover, *Rarg*<sup>-/-</sup> embryos resist the effects of RA toxicity on caudal development, suggesting that RAR $\gamma$  mediates ectopic RA signaling in the tail bud (Lohnes et al., 1993). However, although caudal development proceeds normally in *Cyp26a1*<sup>-/-</sup>*Rarg*<sup>-/-</sup> animals, ablation of *Rarg* does not rescue all defects characterized in *Cyp26a1*<sup>-/-</sup> mutants. In particular, the double mutants retain several vertebral posterior transformations in the cervical region (Fig. 2; Table 2), thus implicating other RARs in mediating the effects of ectopic RA after loss of CYP26A1 function.

### *Cyp26a1* prevents RAR $\gamma$ -mediated disruption of WNT3A and FGF8 signaling pathways

Removal of RAR $\gamma$  function rescues *Wnt3a* and *Fgf8* expression, as well as normal tail bud development, in *Cyp26a1*<sup>-/-</sup> mutants. Both *Fgf8* and *Wnt3a* genes exhibit markedly reduced expression domains in the caudal region of *Cyp26a1*<sup>-/-</sup> embryos (Fig. 4) (Abu-Abed et al., 2001; Sakai et al., 2001). These abnormal transcript patterns could result from

a combination of two events: (1) an impaired development of the tail bud tissues that normally express these genes; and (2) a downregulation of their expression levels (see Fig. 5B for *Fgf8*) [see Sakai et al. (Sakai et al., 2001) for *Wnt3a*]. As a result, impaired FGF8 and WNT3A signaling is likely to affect the tail bud gastrulation movements in *Cyp26a1*<sup>-/-</sup> embryos. In *Wnt3a*<sup>-/-</sup> and *Fgf8*<sup>-/-</sup> mutants, epiblast cells appear to undergo the gastrulation epithelial-to-mesenchymal transition, but fail to migrate laterally or to contribute to mesoderm and endoderm formation (Sun et al., 1999; Takada et al., 1994; Yamaguchi et al., 1999). Furthermore, similar to what we observed in *Cyp26a1*<sup>-/-</sup> embryos, *Wnt3a*<sup>-/-</sup> and *Fgf8*<sup>-/-</sup> mutants show decreased *Brachyury* (Fig. 4) and *Tbx6* (data not shown) expression (Sun et al., 1999; Yamaguchi et al., 1999). The *Fgf8*<sup>-/-</sup>, *Brachyury*<sup>-/-</sup> and *Tbx6*<sup>-/-</sup> abnormal phenotypes are more severe than those observed in *Wnt3a*<sup>-/-</sup> and *Cyp26a1*<sup>-/-</sup> mutant embryos, with severity of the null mutant phenotypes appearing to correspond to onset of their respective gene expression in the tail bud (Chapman and Papaioannou, 1998; Yamaguchi et al., 1999; Yoshikawa et al., 1997). As tail bud defects in CYP26A1 mutants are mediated by RAR $\gamma$ , which only first appears in the caudal embryonic germ layers at E8.0, they should accordingly be less severe than those observed in *Wnt3a*<sup>-/-</sup> embryos. *Cyp26a1*<sup>-/-</sup> fetuses indeed develop thoracic vertebrae, as well as some lumbosacral vertebral remnants, whereas *Wnt3a*<sup>-/-</sup> animals show loss of all vertebrae and tissues caudal to the forelimbs. Thus, our results show that, in the absence of CYP26A1, RAR $\gamma$  downregulates WNT3A and FGF8 signaling (Fig. 7B).

WNT3A and FGF8 are thought to affect the expression of other common targets, such as caudal-related genes, which regulate Hox expression in *Drosophila*, *Xenopus* and mouse (Ikeya and Takada, 2001; Isaacs et al., 1998; Lickert et al., 2000; Northrop and Kimelman, 1994; Prinos et al., 2001). *Cdx4* expression is strongest in the tail bud at a time when 5' Hox genes, which are believed to define identity of more caudal body segments, are first expressed (Burke et al., 1995; Gamer and Wright, 1993). Therefore, we investigated *Cdx4* and *Hoxd11* expression. Our results demonstrate that loss of WNT3A and FGF8 signaling in *Cyp26a1*<sup>-/-</sup> mutants coincides with downregulation of both *Cdx4* and *Hoxd11*. Interestingly, *Hoxd11* expression expanded ventrally in mutants lacking *Rarg*. A similar phenomenon was observed in animals harboring a mutation in a 3' repressor region of the *Hoxd11* gene (Gérard et al., 1996). Together with our results, these observations suggest that in the absence of RA, RAR $\gamma$  may repress *Hoxd11* gene activity in the ventral mesoderm by binding to its 3' repressor element, thereby defining its rostral boundary of expression. As almost normal *Cdx4* and *Hoxd11* expression is restored in *Cyp26a1*<sup>-/-</sup>*Rarg*<sup>-/-</sup> double mutants, ectopic RA signaling through RAR $\gamma$  in the tail bud appears to affect directly and/or indirectly the expression of additional downstream targets of WNT3A and FGF8 signaling, such as the *Cdx* and 5' Hox genes (Fig. 7).

### What is the function of *Rarg* in the tail bud?

Ablation of *Rarg* restored normal gene expression patterns and essentially alleviated caudal regression in *Cyp26a1*<sup>-/-</sup>*Rarg*<sup>-/-</sup> double mutants. What then, besides the possible setting of the rostral boundary of expression of *Hoxd11*, is the physiological function of RAR $\gamma$  in the caudal embryo, and why are *Cyp26a1*

and *Rarg* co-expressed in the tail bud? Loss of RAR $\gamma$  function severely compromises male fertility, by disrupting normal differentiation of glandular epithelia in the seminal vesicles and prostate glands (Lohnes et al., 1993; Look et al., 1995). We note that *Cyp26a1*<sup>-/-</sup>*Rarg*<sup>-/-</sup> double mutant males and females also fail to reproduce normally (data not shown). Thus, as *Cyp26a1*<sup>-/-</sup> males and females in which one *Raldh2* allele has been ablated are fertile (Niederreither et al., 2002a), RAR $\gamma$ -mediated RA-signaling is likely to perform an essential role at some stage in the ontogeny of reproductive organs.

### Reducing RA synthesis or blocking *Rarg*-mediated RA signaling can rescue *Cyp26a1* mutants

RALDH2 and CYP26A1, respectively, show complementary RA-synthesizing and -catabolizing activities throughout embryonic development in several tissues undergoing morphogenesis (Abu-Abed et al., 2002; Fujii et al., 1997; MacLean et al., 2001; Niederreither et al., 1997), enzymatic activities which are conserved in the trunk and tail bud of both mouse and chick embryos (Berggren et al., 1999; Swindell et al., 1999). Our present data indicate that by catabolizing RA, which diffuses from neighboring trunk somites, CYP26A1 activity prevents ectopic RAR $\gamma$ -mediated RA signaling in the tail bud. Interestingly, using a *lacZ*-RA-reporter transgene it has been shown that under *Raldh2*-haploinsufficient conditions the extent of RA diffusion into caudal tissues is reduced, which in turn rescues *Cyp26a1*-null mutant mouse fetuses from lethality (Niederreither et al., 2002a). These observations suggest that below a certain threshold, RA synthesis in the trunk does not interfere with tail bud development (Perlmann, 2002), even in the presence of RAR $\gamma$ . In this respect we note that, although RA treatments downregulate *Raldh2* expression in the trunk (Niederreither et al., 1997), *Cyp26a1* gene expression is induced by RA in the tail bud and craniofacial regions (Iulianella et al., 1999), indicating that feedback responses may have evolved to regulate local RA concentrations. Moreover, we have previously shown that RA-induced *Cyp26a1* expression is mediated by RAR $\gamma$  (Abu-Abed et al., 1998), and, therefore, RAR $\gamma$  may be involved in regulating *Cyp26a1* expression in the tail bud when endogenous RA levels exceed a certain threshold. Thus, it is only in the absence of CYP26A1 or following administration of excess RA, that RAR $\gamma$ -mediated RA signaling becomes lethal by suppressing the expression of genes that control tail bud morphogenesis.

Previously, several mechanisms of partial genetic suppression of lethal null mutations have been reported in the mouse (Kodera et al., 2002; Litingtung and Chiang, 2000; Niederreither et al., 2002a; Tsai et al., 1998). Our present double mutants, in which a *Rarg*-null background rescues caudal regression and neural tube defects in *Cyp26a1*<sup>-/-</sup> mutants, provides a clear illustration of genetic suppression of a lethal mutation, as the ablation of *Rarg*<sup>-/-</sup> allows *Cyp26a1*<sup>-/-</sup> mutants to survive lethal RA levels. Finally, it is interesting to note that in their characterization of mouse models with neural tube defects, Juriloff and Harris (Juriloff and Harris, 2000) identified several genes whose mutational phenotypes are affected by nutritional factors. Supplementation of curly tail mice with inositol or of splotch (*Pax3*) mutants with folic acid reduced the incidence of spina bifida in both types of animals. Our previous (Niederreither et al., 2002a) and present double-

mutant mouse models similarly demonstrate that alterations in RA availability have marked effects on the incidence of spina bifida, and defects of caudal morphogenesis and neural tube formation. Whether similar human congenital defects could result from dysregulation of mechanisms that control the levels of RA remains to be determined.

We thank Drs K. Niederreither, D. Lohnes and A. Tahayato, and Mr K. Young for useful discussions. This work was supported by the Canadian Institutes of Health Research (CIHR) and the National Cancer Institute of Canada (M. P.), as well as institutional funds by CNRS, INSERM, Collège de France, Hôpitaux Universitaires de Strasbourg, Association pour la Recherche sur le Cancer, Fondation pour la Recherche Médicale and Bristol-Myers Squibb (P. D., D. M. and P. C.). S. A.-A. holds a studentship from CIHR.

## REFERENCES

- Abu-Abed, S. S., Beckett, B. R., Chiba, H., Chithalen, J. V., Jones, G., Metzger, D., Chambon, P. and Petkovich, M. (1998). Mouse P450RAI (CYP26) expression and retinoic acid-inducible retinoic acid metabolism in F9 cells are regulated by retinoic acid receptor gamma and retinoid X receptor alpha. *J. Biol. Chem.* **273**, 2409-2415.
- Abu-Abed, S., Dollé, P., Metzger, D., Beckett, B., Chambon, P. and Petkovich, M. (2001). The retinoic acid-metabolizing enzyme, CYP26A1, is essential for normal hindbrain patterning, vertebral identity, and development of posterior structures. *Genes Dev.* **15**, 226-240.
- Abu-Abed, S., MacLean, G., Fraulob, V., Chambon, P., Petkovich, M. and Dollé, P. (2002). Differential expression of the retinoic acid-metabolizing enzymes CYP26A1 and CYP26B1 during murine organogenesis. *Mech. Dev.* **110**, 173-177.
- Alles, A. J. and Sulik, K. K. (1990). Retinoic acid-induced spina bifida: evidence for a pathogenetic mechanism. *Development* **108**, 73-81.
- Ang, S. L., Wierda, A., Wong, D., Stevens, K. A., Cascio, S., Rossant, J. and Zaret, K. S. (1993). The formation and maintenance of the definitive endoderm lineage in the mouse: involvement of HNF3/forkhead proteins. *Development* **119**, 1301-1315.
- Beddington, R. S. and Robertson, E. J. (1999). Axis development and early asymmetry in mammals. *Cell* **96**, 195-209.
- Berggren, K., McCaffery, P., Drager, U. and Forehand, C. J. (1999). Differential distribution of retinoic acid synthesis in the chicken embryo as determined by immunolocalization of the retinoic acid synthetic enzyme, RALDH-2. *Dev. Biol.* **210**, 288-304.
- Burke, A. C., Nelson, C. E., Morgan, B. A. and Tabin, C. (1995). Hox genes and the evolution of vertebrate axial morphology. *Development* **121**, 333-346.
- Chambon, P. (1996). A decade of molecular biology of retinoic acid receptors. *FASEB J.* **10**, 940-954.
- Chapman, D. L. and Papaioannou, V. E. (1998). Three neural tubes in mouse embryos with mutations in the T-box gene Tbx6. *Nature* **391**, 695-697.
- Crossley, P. H. and Martin, G. R. (1995). The mouse Fgf8 gene encodes a family of polypeptides and is expressed in regions that direct outgrowth and patterning in the developing embryo. *Development* **121**, 439-451.
- de Roos, K., Sonneveld, E., Compaan, B., ten Berge, D., Durston, A. J. and van der Saag, P. T. (1999). Expression of retinoic acid 4-hydroxylase (CYP26) during mouse and *Xenopus laevis* embryogenesis. *Mech. Dev.* **82**, 205-211.
- Durston, A. J., van der Wees, J., Pijnappel, W. W., Schilthuis, J. G. and Godsave, S. F. (1997). Retinoid signalling and axial patterning during early vertebrate embryogenesis. *Cell Mol. Life Sci.* **53**, 339-349.
- Favier, B. and Dollé, P. (1997). Developmental functions of mammalian Hox genes. *Mol. Hum. Reprod.* **3**, 115-131.
- Fujii, H., Sato, T., Kaneko, S., Gotoh, O., Fujii-Kuriyama, Y., Osawa, K., Kato, S. and Hamada, H. (1997). Metabolic inactivation of retinoic acid by a novel P450 differentially expressed in developing mouse embryos. *EMBO J.* **16**, 4163-4173.
- Gamer, L. W. and Wright, C. V. (1993). Murine Cdx-4 bears striking similarities to the *Drosophila* caudal gene in its homeodomain sequence and early expression pattern. *Mech. Dev.* **43**, 71-81.
- Gérard, M., Chen, J. Y., Gronemeyer, H., Chambon, P., Duboule, D. and Zakany, J. (1996). In vivo targeted mutagenesis of a regulatory element required for positioning the Hoxd-11 and Hoxd-10 expression boundaries. *Genes Dev.* **10**, 2326-2334.
- Griffith, C. M. and Wiley, M. J. (1991). Effects of retinoic acid on chick tail bud development. *Teratology* **43**, 217-224.
- Herrmann, B. G., Labeit, S., Poustka, A., King, T. R. and Lehrach, H. (1990). Cloning of the T gene required in mesoderm formation in the mouse. *Nature* **343**, 617-622.
- Holleman, T., Chen, Y., Grunz, H. and Pieler, T. (1998). Regionalized metabolic activity establishes boundaries of retinoic acid signalling. *EMBO J.* **17**, 7361-7372.
- Ikeya, M. and Takada, S. (2001). Wnt-3a is required for somite specification along the anteroposterior axis of the mouse embryo and for regulation of cdx-1 expression. *Mech. Dev.* **103**, 27-33.
- Isaacs, H. V., Pownall, M. E. and Slack, J. M. (1998). Regulation of Hox gene expression and posterior development by the *Xenopus* caudal homologue Xcad3. *EMBO J.* **17**, 3413-3427.
- Iulianella, A. and Lohnes, D. (1997). Contribution of retinoic acid receptor gamma to retinoid-induced craniofacial and axial defects. *Dev. Dyn.* **209**, 92-104.
- Iulianella, A., Beckett, B., Petkovich, M. and Lohnes, D. (1999). A molecular basis for retinoic acid-induced axial truncation. *Dev. Biol.* **205**, 33-48.
- Juriloff, D. M. and Harris, M. J. (2000). Mouse models for neural tube closure defects. *Hum. Mol. Genet.* **9**, 993-1000.
- Kessel, M. (1992). Respecification of vertebral identities by retinoic acid. *Development* **115**, 487-501.
- Kinder, S. J., Tsang, T. E., Quinlan, G. A., Hadjantonakis, A. K., Nagy, A. and Tam, P. P. (1999). The orderly allocation of mesodermal cells to the extraembryonic structures and the anteroposterior axis during gastrulation of the mouse embryo. *Development* **126**, 4691-4701.
- Kodera, T., McGaha, T. L., Phelps, R., Paul, W. E. and Bona, C. A. (2002). Disrupting the IL-4 gene rescues mice homozygous for the tight-skin mutation from embryonic death and diminishes TGF-beta production by fibroblasts. *Proc. Natl. Acad. Sci. USA* **99**, 3800-3805.
- Lickert, H., Dorn, C., Huls, G., Wehrle, C., Duluc, L., Clevers, H., Meyer, B. I., Freund, J. N. and Kemler, R. (2000). Wnt/(beta)-catenin signaling regulates the expression of the homeobox gene Cdx1 in embryonic intestine. *Development* **127**, 3805-3813.
- Litingtung, Y. and Chiang, C. (2000). Specification of ventral neuron types is mediated by an antagonistic interaction between Shh and Gli3. *Nat. Neurosci.* **3**, 979-985.
- Lohnes, D., Kastner, P., Dierich, A., Mark, M., LeMeur, M. and Chambon, P. (1993). Function of retinoic acid receptor gamma in the mouse. *Cell* **73**, 643-658.
- Lohnes, D., Mark, M., Mendelsohn, C., Dollé, P., Dierich, A., Gorry, P., Gansmuller, A. and Chambon, P. (1994). Function of the retinoic acid receptors (RARs) during development (I). Craniofacial and skeletal abnormalities in RAR double mutants. *Development* **120**, 2723-2748.
- Look, J., Landwehr, J., Bauer, F., Hoffmann, A. S., Bluethmann, H. and LeMotte, P. (1995). Marked resistance of RAR gamma-deficient mice to the toxic effects of retinoic acid. *Am. J. Physiol.* **269**, E91-E98.
- MacLean, G., Abu-Abed, S., Dollé, P., Tahayato, A., Chambon, P. and Petkovich, M. (2001). Cloning of a novel retinoic acid-metabolizing cytochrome P450, Cyp26B1, and comparative expression analysis with Cyp26A1 during early murine development. *Mech. Dev.* **107**, 195-201.
- Mic, F. A., Molotkov, A., Fan, X., Cuenca, A. E. and Duester, G. (2000). RALDH3, a retinaldehyde dehydrogenase that generates retinoic acid, is expressed in the ventral retina, otic vesicle and olfactory pit during mouse development. *Mech. Dev.* **97**, 227-230.
- Monaghan, A. P., Kaestner, K. H., Grau, E. and Schutz, G. (1993). Postimplantation expression patterns indicate a role for the mouse forkhead/HNF-3 alpha, beta and gamma genes in determination of the definitive endoderm, chordamesoderm and neuroectoderm. *Development* **119**, 567-578.
- Niederreither, K., McCaffery, P., Drager, U. C., Chambon, P. and Dollé, P. (1997). Restricted expression and retinoic acid-induced downregulation of the retinaldehyde dehydrogenase type 2 (RALDH-2) gene during mouse development. *Mech. Dev.* **62**, 67-78.
- Niederreither, K., Subbarayan, V., Dollé, P. and Chambon, P. (1999). Embryonic retinoic acid synthesis is essential for early mouse post-implantation development. *Nat. Genet.* **21**, 444-448.
- Niederreither, K., Abu-Abed, S., Schuhbaur, B., Petkovich, M., Chambon, P. and Dollé, P. (2002a). Genetic evidence that oxidative derivatives of

- retinoic acid are not involved in retinoid signaling during mouse development. *Nat. Genet.* **15**, 84-88.
- Niederreither, K., Fraulob, V., Garnier, J. M., Chambon, P. and Dollé, P.** (2002b). Differential expression of retinoic acid-synthesizing (RALDH) enzymes during fetal development and organ differentiation in the mouse. *Mech. Dev.* **110**, 165-171.
- Northrop, J. L. and Kimelman, D.** (1994). Dorsal-ventral differences in Xcad-3 expression in response to FGF-mediated induction in *Xenopus*. *Dev. Biol.* **161**, 490-503.
- Padmanabhan, R.** (1998). Retinoic acid-induced caudal regression syndrome in the mouse fetus. *Reprod. Toxicol.* **12**, 139-151.
- Parr, B. A., Shea, M. J., Vassileva, G. and McMahon, A. P.** (1993). Mouse Wnt genes exhibit discrete domains of expression in the early embryonic CNS and limb buds. *Development* **119**, 247-261.
- Perlmann, T.** (2002). Retinoid metabolism: a balancing act. *Nat. Genet.* **15**, 1-2.
- Pownall, M. E., Tucker, A. S., Slack, J. M. and Isaacs, H. V.** (1996). eFGF, Xcad3 and Hox genes form a molecular pathway that establishes the anteroposterior axis in *Xenopus*. *Development* **122**, 3881-3892.
- Prinos, P., Joseph, S., Oh, K., Meyer, B. I., Gruss, P. and Lohnes, D.** (2001). Multiple pathways governing Cdx1 expression during murine development. *Dev. Biol.* **239**, 257-269.
- Roelink, H. and Nusse, R.** (1991). Expression of two members of the Wnt family during mouse development—restricted temporal and spatial patterns in the developing neural tube. *Genes Dev.* **5**, 381-388.
- Rossant, J., Zirngibl, R., Cado, D., Shago, M. and Giguère, V.** (1991). Expression of a retinoic acid response element-hsplacZ transgene defines specific domains of transcriptional activity during mouse embryogenesis. *Genes Dev.* **5**, 1333-1344.
- Ruberte, E., Dollé, P., Krust, A., Zelent, A., Morriss-Kay, G. and Chambon, P.** (1990). Specific spatial and temporal distribution of retinoic acid receptor gamma transcripts during mouse embryogenesis. *Development* **108**, 213-222.
- Ruiz i Altaba, A. and Jessell, T.** (1991). Retinoic acid modifies mesodermal patterning in early *Xenopus* embryos. *Genes Dev.* **5**, 175-187.
- Sakai, Y., Meno, C., Fujii, H., Nishino, J., Shiratori, H., Saijoh, Y., Rossant, J. and Hamada, H.** (2001). The retinoic acid-inactivating enzyme CYP26 is essential for establishing an uneven distribution of retinoic acid along the antero-posterior axis within the mouse embryo. *Genes Dev.* **15**, 213-225.
- Sasaki, H. and Hogan, B. L.** (1993). Differential expression of multiple fork head related genes during gastrulation and axial pattern formation in the mouse embryo. *Development* **118**, 47-59.
- Shum, A. S., Poon, L. L., Tang, W. W., Koide, T., Chan, B. W., Leung, Y. C., Shiroishi, T. and Copp, A. J.** (1999). Retinoic acid induces down-regulation of Wnt-3a, apoptosis and diversion of tail bud cells to a neural fate in the mouse embryo. *Mech. Dev.* **84**, 17-30.
- Simeone, A., Avantaggiato, V., Moroni, M. C., Mavilio, F., Arra, C., Cotelli, F., Nigro, V. and Acampora, D.** (1995). Retinoic acid induces stage-specific antero-posterior transformation of rostral central nervous system. *Mech. Dev.* **51**, 83-98.
- Subramanian, V., Meyer, B. I. and Gruss, P.** (1995). Disruption of the murine homeobox gene *Cdx1* affects axial skeletal identities by altering the mesodermal expression domains of Hox genes. *Cell* **83**, 641-653.
- Sun, X., Meyers, E. N., Lewandoski, M. and Martin, G. R.** (1999). Targeted disruption of *Fgf8* causes failure of cell migration in the gastrulating mouse embryo. *Genes Dev.* **13**, 1834-1846.
- Swindell, E. C., Thaller, C., Sockanathan, S., Petkovich, M., Jessell, T. M. and Eichele, G.** (1999). Complementary domains of retinoic acid production and degradation in the early chick embryo. *Dev. Biol.* **216**, 282-296.
- Takada, S., Stark, K. L., Shea, M. J., Vassileva, G., McMahon, J. A. and McMahon, A. P.** (1994). Wnt-3a regulates somite and tailbud formation in the mouse embryo. *Genes Dev.* **8**, 174-189.
- Tsai, K. Y., Hu, Y., Macleod, K. F., Crowley, D., Yamasaki, L. and Jacks, T.** (1998). Mutation of E2f-1 suppresses apoptosis and inappropriate S phase entry and extends survival of Rb-deficient mouse embryos. *Mol. Cell* **2**, 293-304.
- Ulven, S. M., Gundersen, T. E., Weedon, M. S., Landaas, V. O., Sakhi, A. K., Fromm, S. H., Geronimo, B. A., Moskaug, J. O. and Blomhoff, R.** (2000). Identification of endogenous retinoids, enzymes, binding proteins, and receptors during early postimplantation development in mouse: important role of retinal dehydrogenase type 2 in synthesis of all-trans-retinoic acid. *Dev. Biol.* **220**, 379-391.
- Wilkinson, D. G.** (1992). *In Situ Hybridization: A Practical Approach*. Oxford, UK: IRL Press.
- Yamaguchi, T. P., Takada, S., Yoshikawa, Y., Wu, N. and McMahon, A. P.** (1999). T (Brachyury) is a direct target of Wnt3a during paraxial mesoderm specification. *Genes Dev.* **13**, 3185-3190.
- Yasuda, Y., Konishi, H., Kihara, T. and Tanimura, T.** (1990). Discontinuity of primary and secondary neural tube in spina bifida induced by retinoic acid in mice. *Teratology* **41**, 257-274.
- Yoshikawa, Y., Fujimori, T., McMahon, A. P. and Takada, S.** (1997). Evidence that absence of Wnt-3a signaling promotes neuralization instead of paraxial mesoderm development in the mouse. *Dev. Biol.* **183**, 234-242.